Proceedings of CONF-MLA 2026 Symposium: Intelligent Systems and Automation: AI Models, IoT, and Robotic Algorithms
DOI: 10.54254/2755-2721/2026.LD36578

Time Difference of Arrival Localization Based on Ultra-Wideband: A Synergistic Method of System and Algorithm II

Yulin Rao, Kaitao Wen, Paul Brennan*

Engineering (Electronic and Electrical), University College London, London, UK
**Corresponding Author. Email: p.brennan@ucl.ac.uk*

Abstract. Following the previous study of TDoA localization algorithms and hardware-assisted calibration, this paper develops a configurable DW1000-based ultra-wideband (UWB) platform for indoor localization with multiple anchors. Dedicated PCBs for the anchor and tag were designed to combine the DW1000 transceiver, STM32 controller interface, regulated power supply, controlled RF path, and customized antenna in one module. Three antenna candidates, including a modified circular radiator, a conventional circular patch, and a rectangular patch, were modelled in CST Studio Suite under the same conditions using a 1.2-mm F4B substrate. With the -6 dB level used as the preliminary comparison standard, the modified circular radiator obtained the widest simulated range from 6.0313 to 6.4318 GHz, giving an approximate bandwidth of 400.5 MHz. However, its -10 dB impedance bandwidth still requires further optimization before the antenna can be fabricated. The software was divided into three layers: an STM32 driver layer, a DW1000 API layer, and an application layer. This structure supports radio configuration, packet transmission and reception, timestamp reading, and future TDoA implementation. An infrared-synchronized ultrasonic unit was also developed as an additional short-range reference. It can be used to investigate UWB bias and to provide an initial region for the Taylor-series estimator. Nevertheless, one ultrasonic distance cannot independently determine a two-dimensional position or remove the clock drift between anchors. Qualitative tests were also carried out for multipath propagation, obstacle blockage, antenna orientation, and nearby wireless activity. These tests indicate several practical risks for system installation and provide a hardware and firmware basis for future synchronized multi-anchor experiments and quantitative localization evaluation.

Keywords: STM-32 processors, CST studio, patch antenna, Coax feed, Microstrip-Line Feed

1. Introduction

Indoor localization is important for mobile robots, automated transport platforms and warehouse vehicles, especially when GPS signals are unavailable or cannot provide a reliable result. Ultra-wideband (UWB) technology [1] is a suitable choice for these applications because it uses short-duration pulses and a wide operating bandwidth to obtain accurate timing information. In a favourable line-of-sight environment, this high time resolution can support precise range and short-range position estimation. However, the final performance of a Time Difference of Arrival (TDoA)

DOI: 10.54254/2755-2721/2026.LD36578

system does not only depend on the localization algorithm. Timestamp stability, clock synchronization between anchors, antenna propagation delay, PCB layout, and indoor multipath conditions can all introduce errors into the measured arrival-time differences. Therefore, a suitable hardware platform is required before the improvement of the algorithm can be transferred into a practical embedded localization system.

The previous part of this work [2] established the mathematical model of the TDoA method and compared Fang's, Chan's, and Taylor-series-based algorithms. Commercial ESP32-DW1000 modules were also used for preliminary ranging calibration and two-anchor geometric positioning. The results showed that Taylor-series refinement can provide a useful correction process, but its convergence is strongly affected by the measurement bias and the quality of the initial position. Although commercial ESP32-DW1000 modules [3] are convenient for fast testing, their fixed antenna structures, predefined PCB layouts and limited wired interfaces make it difficult to optimize the RF section or connect the module directly with an external vehicle controller.

This paper is based on previous study by developing a configurable DW1000-based UWB hardware platform for multi-anchor localization system. It includes multiple anchors and tag PCB layouts, an STM32 MCU, a DW1000 interface, and an integrated antenna design. The emphasis is placed on module integration, antenna selection, firmware organization, and practical deployment factors rather than repeating the TDoA derivation presented previously.

The main work includes four sections. First, seperate anchors and tags PCB designs are developed with their ownpower, SPI communication, hardware reset and interrupt connections, controlled RF routing and an external wired interface. Second, three individual antenna structures are modelled and tested in CST Studio Suite. Third, a three-layer firmware structure is implemented for the STM32, DW1000 API and application functions. Lastly, an infrared-synchronized with an ultrasonic unit and several qualitative tests are introduced to examine UWB bias, initial-position estimation, multipath, obstacle blockage, antenna orientation and nearby wireless activity. Vehicle navigation, obstacle avoidance and motor control remain outside the scope of this paper.

2. Overview for the system and the requirements for design

The proposed system is a modular UWB localization subsystem designed for integration with an external embedded platform. Its main functions are to transmit and receive UWB frames, generate and retrieve hardware timestamps, and provide measurement data for multi-anchor position estimation. Localization hardware is separated from vehicle navigation and motor-control functions so that the same module can be reused across different platforms.

2.1. System architecture and node roles

As Figure 1 illustrates, each node contains two DW1000 transceivers, a regulated power section, reset and interrupt connections, an RF feed network, an antenna, and an SPI interface to an STM32 controller [4]. The DW1000 devices perform UWB transmission, reception, and hardware timestamp generation. The STM32 configures the radios, controls packet exchange, retrieves timestamps, and transfers measurement data or processed results through a wired interface. It acts as the local radio controller, while any higher-level vehicle controller is treated as an external device.

DOI: 10.54254/2755-2721/2026.LD36578

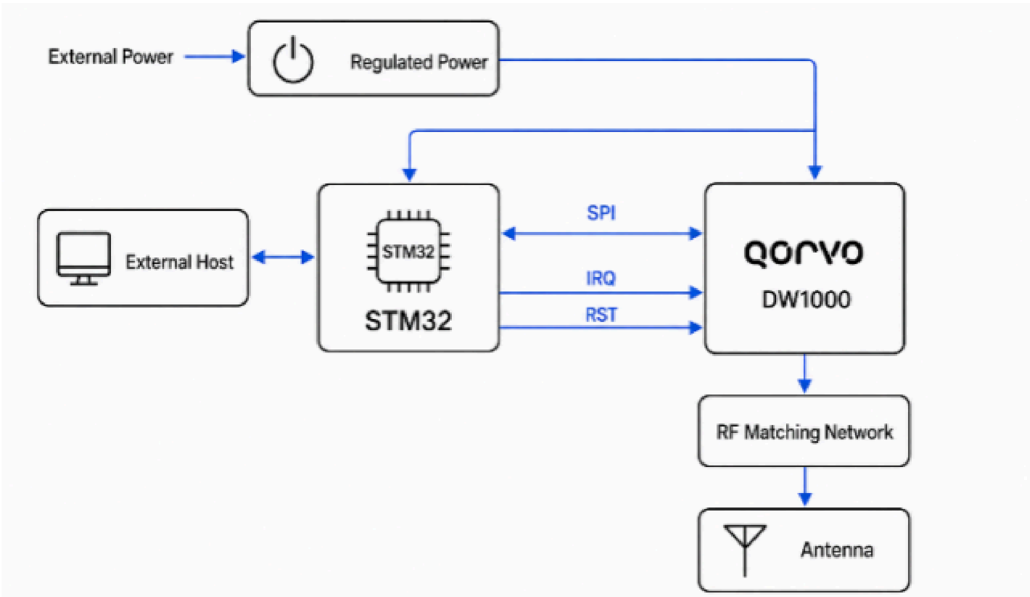

Figure 1. Architecture of the platform

The intended network contains multiple fixed anchors at known coordinates and at least one mobile tag. In the TDoA configuration considered here, the tag transmits a UWB packet that is received and timestamped by the anchors. Differences between the recorded arrival times are supplied to the localization processor to estimate the tag position. Removing synchronization between the tag and anchors does not remove the requirement for a common or compensated time reference among the anchors. The proposed module therefore provides the radio, timestamp, and processing interfaces required for TDoA deployment, while a complete anchor-synchronization method must be developed separately [5].

Anchor and tag nodes share the same DW1000-based core architecture, reducing the number of unique hardware and firmware components. Their layouts may nevertheless differ according to mounting, power, antenna placement, and external-interface requirements. The dashed path in Figure 1 represents an optional ultrasonic reference used only for short-range characterization and initialization and it is not part of the normal UWB signal path.

2.2. Design requirements and scope

The hardware design for the system was developed according to four basic requirements. First, the module must provide a stable power supply under high-speed SPI communication, reset control, interrupt handling, and access to the DW1000 timestamps. Second, the RF connection is designed for a standard 50 Ω impedance, with a controlled signal route and a clear keep-out area around the antenna. Third, the anchors and tags should use the same basic controller and transceiver functions, while still allowing their PCB layouts and application programs to be regulated for different uses. Finally, a hardware interface is provided so that an external controller can receive the timestamps or the calculated localization results [6].

The ultrasonic sensor is only used for short-range bias testing and for supporting the initial position estimate. An ultrasonic distance measurement cannot determine a unique two-dimensional position. However, when it is combined with a previous position or other measurements, it can reduce the possible initialization area. GPS guidance, LIDAR obstacle avoidance, vehicle dynamics, and motor control are not considered in this paper.

DOI: 10.54254/2755-2721/2026.LD36578

3. Hardware design based on the DW1000 UWB module

This section presents the DW1000 module architecture, PCB integration, and antenna design. Because the DW1000 reference circuit is documented by Decawave, the work focuses on adapting it to the anchor and tag modules, improving the RF layout, and selecting an antenna for indoor localization.

3.1. Module architecture of DW1000 circuit

The core device is the Decawave DW1000 UWB transceiver, which supports UWB transmission, reception, and high-accuracy timestamp generation. The STM32 controller communicates with the DW1000 through SPI and manages radio configuration, data packets, timestamps, and commands from the platform controller. The circuit follows the reference architecture and includes RF, power-supply, reset, and interrupt connections.

Figure 2 and Figure 3 present the controller connection at two levels. Figure 2 shows the functional data and control paths, while Figure 3 gives the corresponding electrical connection. SPI transfers configuration data and timestamps, and the reset and interrupt lines support initialization and event notification.

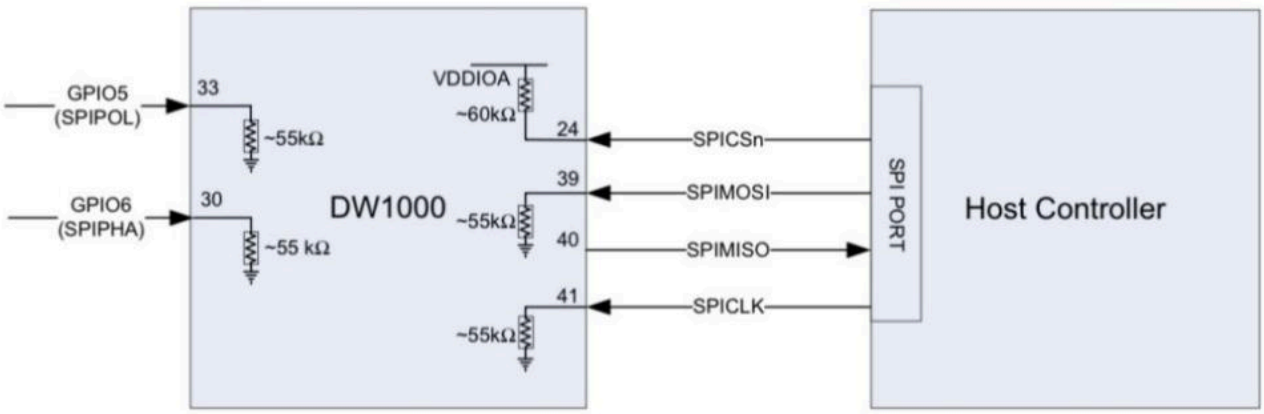

Figure 2. Link between module and MCU

The design of module is based on two types, anchor and tag. The anchor device is used as a fixed reference location in the positioning system, while the tag is carried by the moving vehicle/platform. Both design types share the same DW1000-based core architecture, but their PCB layouts and external connection requirements are adapted to different working conditions. The specialized design also provides a harder connection interface to the MCU than general UWB modules.

DOI: 10.54254/2755-2721/2026.LD36578

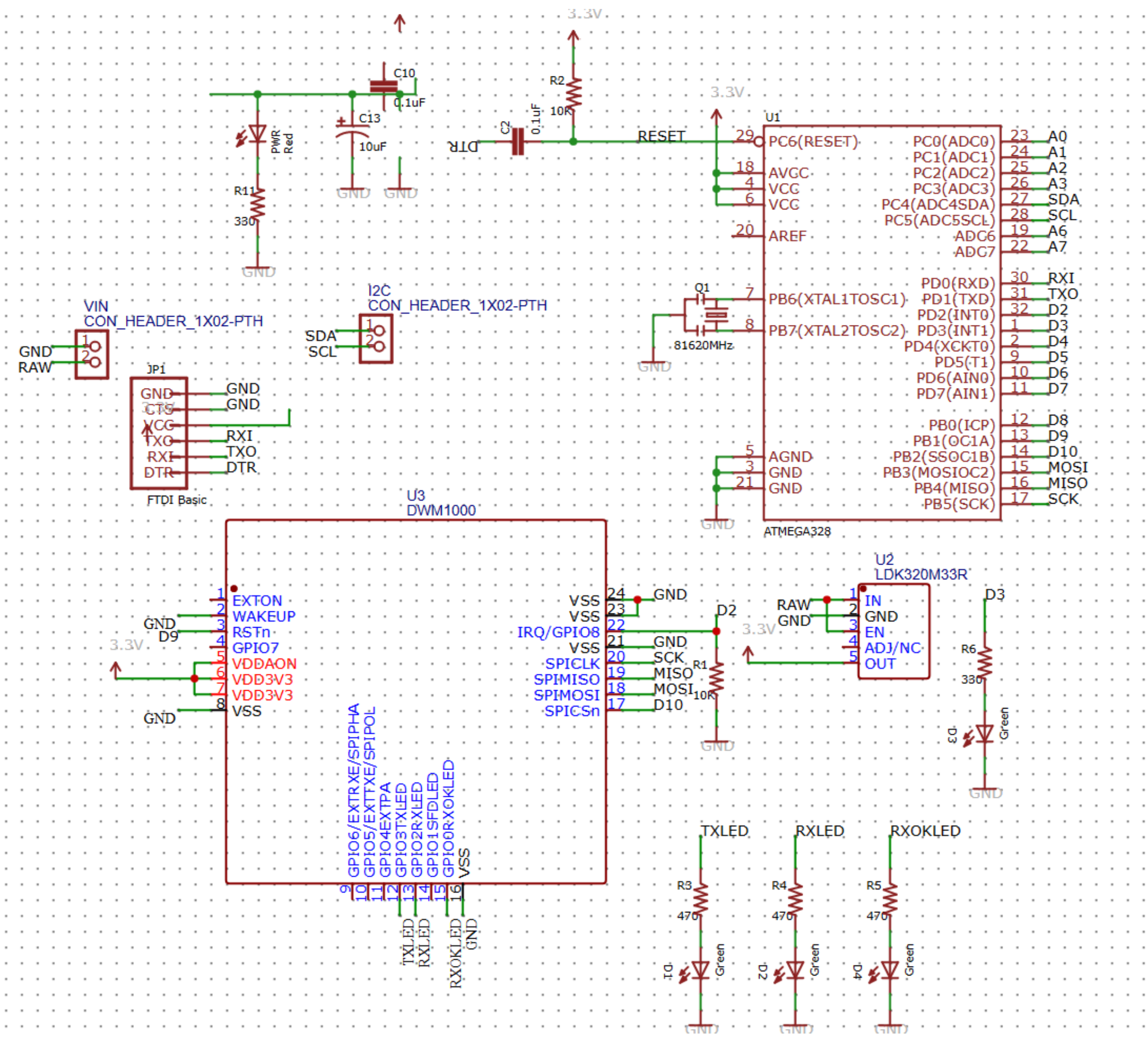

Figure 3. Schematic of the connection

3.2. PCB integration for anchor and tag nodes

Different PCB designs are produced for anchors and tags. The proposal to design a new PCB for the DW1000 module is to integrate the DW1000 module, MCU interface, RF unit (antenna structure) and external communication connector into a single unit module. Different from those general commercial ESP32-based UWB modules, the design provides higher flexibility in antenna special design, module installation and hardware communication with the vehicle platform.

The RF section layout was the most sensitive part of the PCB. The wire route between the DW1000 and the antenna shall control the impedance and reduce the unnecessary breakthrough. Meanwhile, the digital signal and dense wired area shall be kept away from the antenna part to reduce the interference and distortion of the signal received by the antenna. The antenna shall also be placed with sufficient distance from those large components and metal surfaces, especially with those actuators of the vehicle. These layout requirements are especially important for UWB localization because antenna performance directly affects packet reception, timestamp stability and ranging accuracy.

Thereby, based on the criteria we have above, the PCB layout designs for both anchors and tags are shown with Figure 4 and Figure 5.

DOI: 10.54254/2755-2721/2026.LD36578

PCB for Anchor:

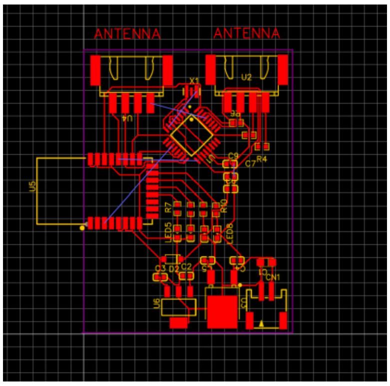

Figure 4. Anchor PCB

PCB for Tag:

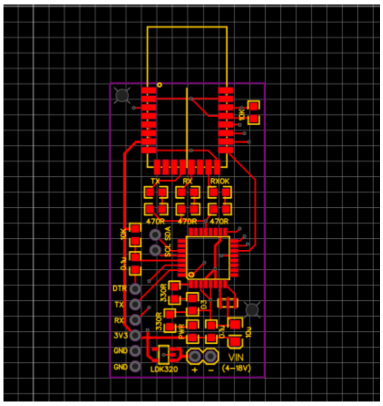

Figure 5. Tag PCB

3.3. Antenna material and feeding method considerations

Substrate material influences antenna size, impedance bandwidth, radiation efficiency, fabrication tolerance and cost. Copper was selected for the radiator because it provides conductivity and can be produced using PCB processes. The dielectric constant and loss tangent affect wavelength, dielectric loss and impedance matching. Although a higher dielectric constant can make the antenna smaller, it may reduce bandwidth and increase fabrication sensitivity. Therefore, a low-loss substrate was preferred for this UWB design.

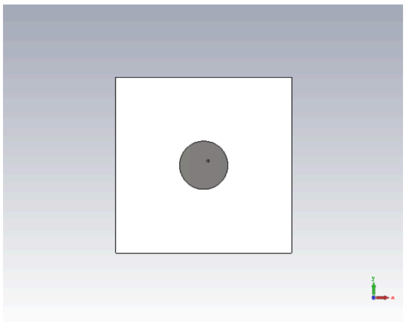

Figure 6. Conventional circular antenna

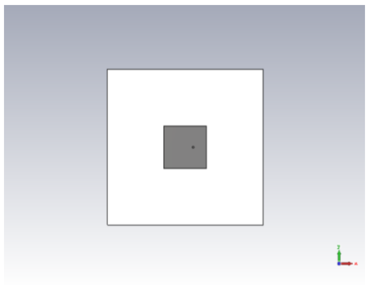

Figure 7. Conventional rectangular antenna

Figure 6 and Figure 7 show the conventional circular and rectangular antennas used as reference structures. The modified circular radiator is presented in Figure 8. A diamond-shaped gap was added to change the surface-current path and adjust its resonant response. Figure 9 shows the related feedline placed on the other side of the substrate. For the CST simulation, a 1.2-mm F4B substrate was selected to balance antenna bandwidth, module size and manufacturing difficulty. A thicker substrate may increase bandwidth, but it can also produce more surface waves and change the radiation pattern.

DOI: 10.54254/2755-2721/2026.LD36578

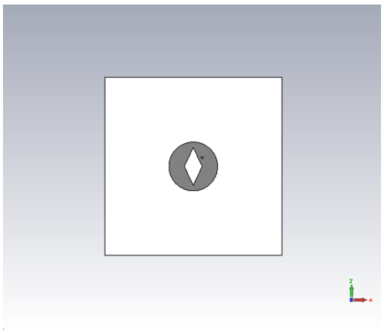

Figure 8. Modified antenna

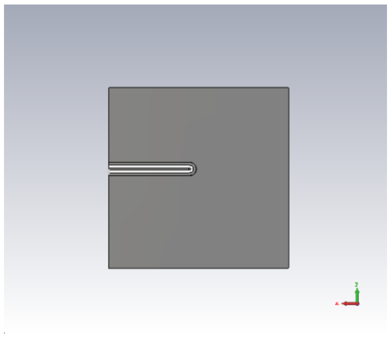

Figure 9. Feedline of modified antenna

Several feeding methods were considered, including coaxial-probe, microstrip-line, aperture-coupled, and proximity-coupled feeds. Coaxial feeding is convenient for antenna testing, whereas aperture and proximity coupling may improve bandwidth at the cost of multilayer fabrication. A microstrip-line feed was selected because it can be fabricated on the module PCB and directly connected to the RF path. Its dimensions were calculated using TXLINE to obtain an initial impedance close to 50 Ω.

3.4. Feedline design and CST modelling

The feedline for the antenna was initially calculated using TXLINE. The target impedance was set to 50 Ω, and the dielectric constant and substrate thickness were defined according to the selected F4B material. The calculated width was transferred to CST and adjusted together with the radiator and ground-plane dimensions [7].

Three candidate structures were constructed: a modified circular antenna, a conventional circular patch, and a rectangular patch. The modified radiator includes a diamond-shaped gap intended to alter its current path and resonance, together with a microstrip feed on the opposite side.

All candidates were simulated using the same substrate and simulation conditions. Reflection coefficients were calculated over 4-8 GHz, and the resulting S-parameter curves were used to compare resonance and approximate bandwidth. Section 3.5 presents the results.

3.5. CST simulation results and selection for the system

The results generated from CST show the reflection coefficients of three candidate antennas presented from Figures 10-12, while the approximate results extracted from the curves charts are summarized in Table 1. The mark we set is -6dB, we will use this level to judge the preliminary operating ranges. The -6 dB threshold is used only as a preliminary comparative criterion for the three simulated geometries. In this case, the performance criteria matching we demonstrate is not conventional -10 dB, instead, compare the influence brought by the antenna geometry.

Table 1. Simulation figures for different antenna patches

Candidate antenna	Approximate resonance	-6 dB frequency range	Approximate -6 dB bandwidth
Adapted circular antenna	6.2 GHz	6.0313–6.4318 GHz	400.5 MHz

DOI: 10.54254/2755-2721/2026.LD36578

Table 1. (continued)

Conventional circular patch	7.0 GHz	6.8695–7.1795 GHz	310.0 MHz
Rectangular patch	6.0 GHz	5.9251–6.1491 GHz	224.0 MHz

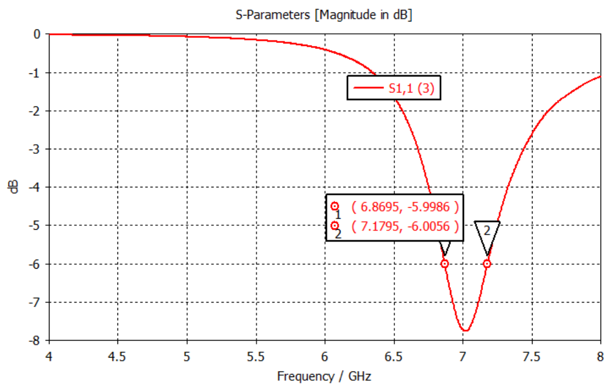

Figure 10. Coefficient for conventional circular antenna

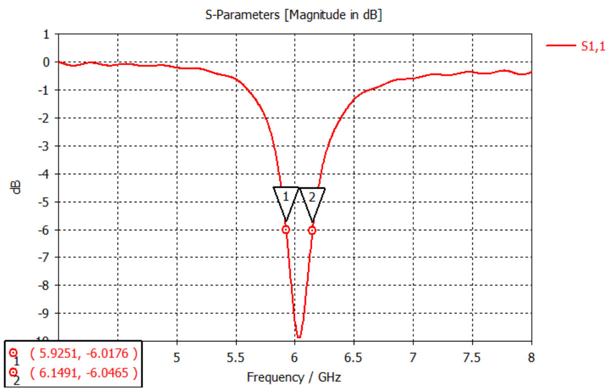

Figure 11. Coefficient for conventional rectangular antenna

As Figure 10 shows, the conventional circular patch produced a resonance at around 7 GHz. The -6dB operation range extended from 6.8695 to 7.1795 GHz, with a bandwidth of around 310 MHz. However, this result was higher than the expected operating region for UWB. The rectangular patch in Figure 11 generated a deeper but narrower operation range at near 6.0 GHz. The operation range extended from 5.9251 to 6.1491 GHz, with an operation bandwidth of around 224 MHz. Although this design provided the strongest resonant response, the operation range is too narrow and makes its performance more sensitive and less robust to environmental factors, fabrication tolerances and PCB integration.

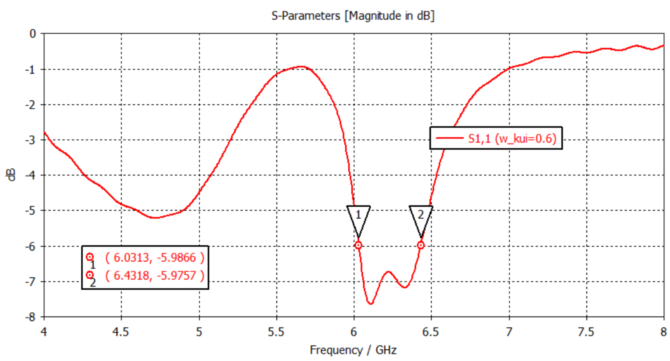

Figure 12. Coefficient formodified circular antenna

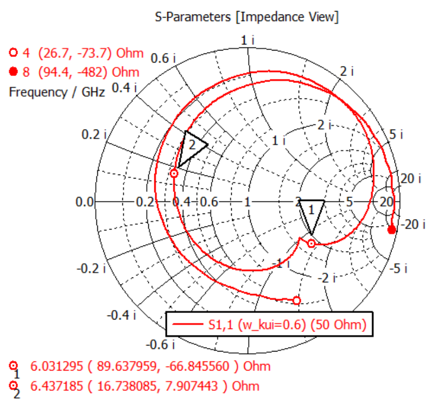

Figure 13. Poles and zeros of modified antenna

For the modified antenna, in Figure 12 its principal resonance occurred at approximately 6.2 GHz, while the operation frequency extended from 6.0313 to 6.4318 GHz, with a resulting operation

DOI: 10.54254/2755-2721/2026.LD36578

bandwidth around 400.5 MHz, which was the widest of three candidate's design. The Smith chart in Figure 13 also demonstrates that the input impedance varied significantly across this frequency range, proving that both the gap within the circle and its feeding structure produce influence for both resistive and reactive parameters.

In this case, the modified circular antenna was used for the UWB system design, because it provided the widest preliminary operation frequency and could be easily integrated into the available PCB layout, as the Figure 14 3.5m-o represented. However, its S-11 parameter still maintains at a level above -10dB. Therefore, it is necessary to make further optimization of the gap designs, feed position and ground-plane geometry before final integration into PCB layout and fabrication of the devices and the experiment demonstration.

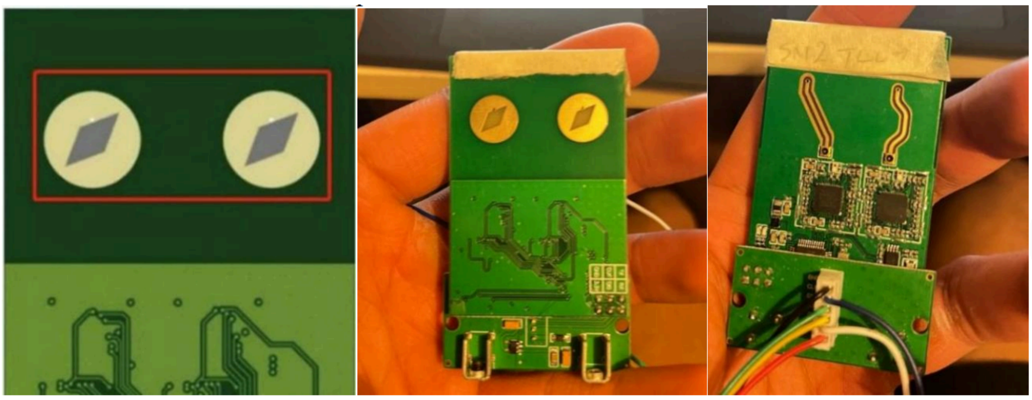

Figure 14. M/n/o prototype of module with modified antenna

4. Hardware testing & simulation

The module firmware was designed to connect the STM32 controller, DW1000 transceiver and localization application without placing all operations in a single program. In addition, an independent ultrasonic unit was developed to provide a short-range reference for UWB bias assessment and Taylor-series initialization.

4.1. Layered firmware implementation

As Figure 15 illustrates, the software configuration consists of three layers: the STM32 driver layer, the DW1000 application programming interface layer and the application layer. The driver layer provides SPI and GPIO functions for chip selection, reset, interrupting handling and data transfer. The STM32 peripherals were initialized using STM32CubeMX, while the Hardware Abstraction Layer was developed in Keil MDK. Above this level, the DW1000 API performs device initialization, radio configuration, frame transmission and reception, and timestamp reading [8]. Hence, the application layer does not need to operate the DW1000 registers directly.

The application program manages anchor–tag communication, packet sequencing, serial output and the interface to the TDoA algorithm. In this case, anchor and tag nodes can reuse the same driver and API functions while applying different communication logic. The software structure and the corresponding execution flow are presented in Figures 15 and Figure 16.

DOI: 10.54254/2755-2721/2026.LD36578

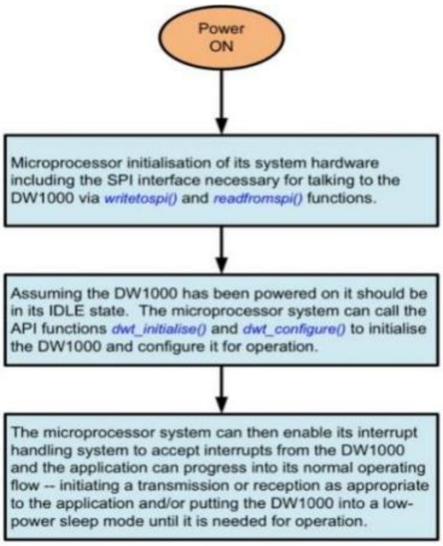

Figure 15. Software layered structure

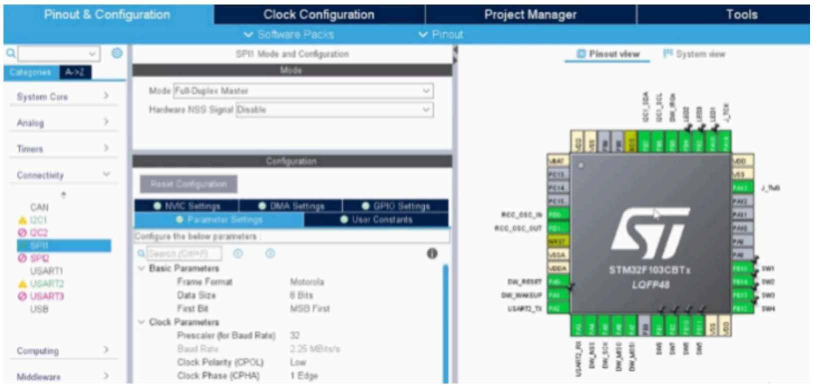

Figure 16. MCU configuration

4.2. Development of the ultrasonic reference unit

The original reference was based on the HC-SR04, which integrates the ultrasonic transmitter and receiver on the same PCB. However, the mobile platform only requires the receiving function, and the unused transmitter may produce acoustic interference [9]. Covering the transmitter and adjusting the trigger sequence were initially tested, but program-execution delay and wireless-trigger uncertainty reduced the repeatability of this method. Therefore, the transmitter and receiver were separated as independent units.

Figure 17 shows the extracted ultrasonic transducer. The receiver outputs without and with an ultrasonic input are compared in Figure 18 and Figure 19. The difference in amplitude provides the basis for threshold detection. Based on this result, the final receiver and transmitter circuits were developed, as shown in Figure 20 and Figure 21.

Figure 17. Signal without signal input

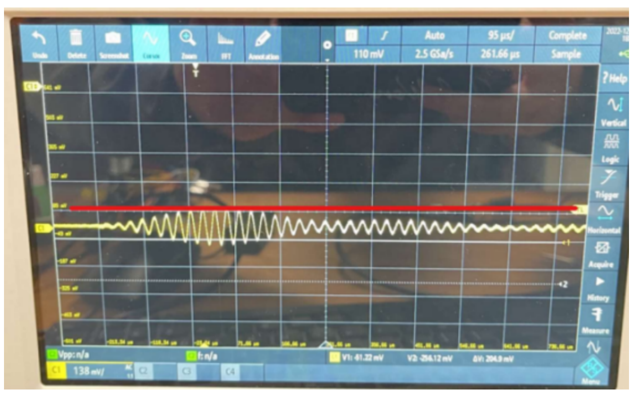

Figure 18. Signal with signal input

DOI: 10.54254/2755-2721/2026.LD36578

Figure 19. Single ultrasonic transducer

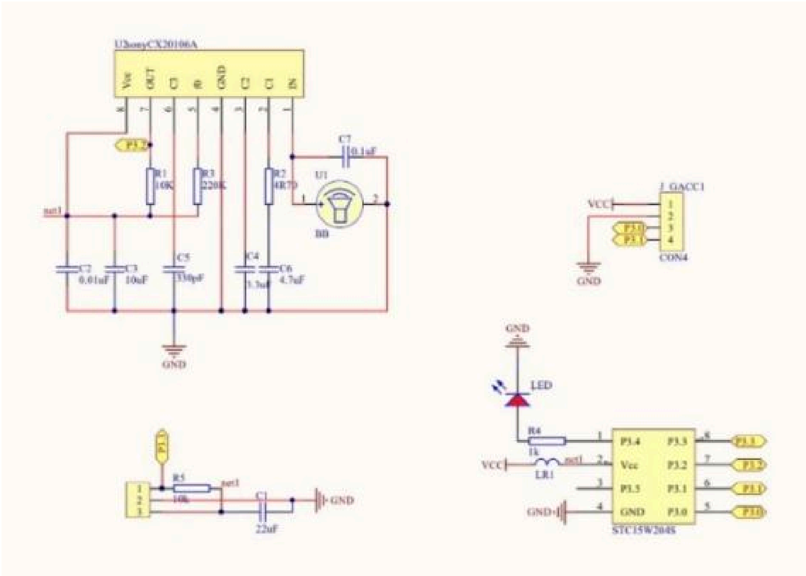

Figure 20. Circuit for receiver

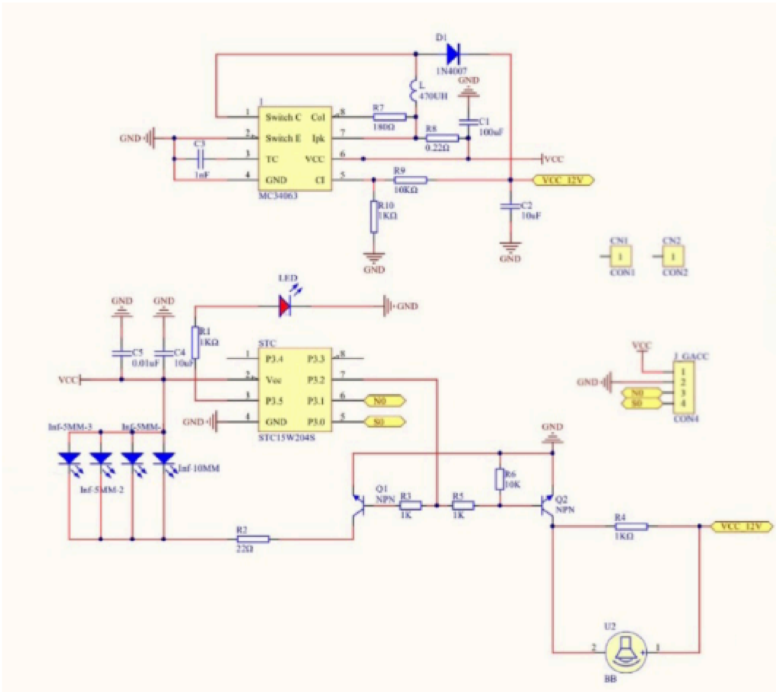

Figure 21. Circuit for transmitter

An infrared pulse is transmitted immediately before the ultrasonic pulse to provide an approximate common start event. The receiver starts timing after detecting the infrared signal and stops when the ultrasonic signal crosses the detection threshold. Since the infrared propagation time is negligible over the tested distance, the one-way reference distance can be approximated by:

$$d_{US} = c_{air} \Delta t_{us} \tag{1}$$

DOI: 10.54254/2755-2721/2026.LD36578

Where d_u is the ultrasonic reference distance c_{air} is the speed of sound in air and Δt_{US} is the measured interval between the infrared and ultrasonic detections. The use of this distance within the UWB system is discussed in Section 4.3.

4.3. Integration with the UWB localization process

The ultrasonic unit is used as an auxiliary reference for the UWB localization process rather than as a replacement for UWB positioning. At a known short-range position, the ultrasonic distance d_u can be compared with a corresponding UWB ranging result d_{UWB}. This comparison can be used to characterize the practical ranging bias b_{UWB}:

$$b_{UWB} = d_{UWB} - d_u \quad (2)$$

The bias term should only be used for compensation after repeated measurements have been performed under controlled conditions. In the present work, the ultrasonic unit is primarily treated as a short-range reference for evaluating the feasibility of this procedure [10].

The ultrasonic measurement can also provide an initial-position constraint for the Taylor-series iterative estimator discussed in the previous study [2]. If the ultrasonic reference is located at p_u, a candidate initial position p_0 should approximately satisfy:

$$\|p_0 - p_u\| \approx d_u \quad (3)$$

This condition defines a circular feasible region in a two-dimensional plane rather than a unique position. It should therefore be combined with a previous position, a known movement direction, or additional measurements before being supplied to the iterative algorithm. The auxiliary ultrasonic measurement can improve the plausibility of the initial estimate, but it does not provide inter-anchor synchronization and cannot compensate for anchor clock offset or drift. The effects of multipath, obstacle blockage, antenna orientation, and wireless activity are discussed in Section 5.

5. Practical performance factors and deployment considerations

The practical performance of a TDoA localization system depends on the propagation environment as well as the antenna, timestamp, and synchronization subsystems. Exploratory tests reported here were used to identify deployment risks for the available UWB prototype. Because repeated ranging errors, packet-loss statistics, and ground-truth position measurements were not recorded, the observations in this section are interpreted qualitatively rather than as a complete localization-performance evaluation.

5.1. Multipath propagation and node placement

Figure 22 and Figure 23 demonstrate the gap between a line-of-sight path and an indoor multipath environment. Many features inside indoor environments like floor, walls, and nearby objects generate delayed signals in addition to the direct path [11]. When the direct incident is attenuated or been blocked, the stronger reflective component might affect first-path detection and introduce a positive timestamp error. This phenomenon is quite crucial for TDoA because the error will significantly change the measured range differences and move the resulted position solution. Therefore, anchors shall be installed with clear propagation paths where possible and separated from large metallic objects, walls, vehicle actuators, and other structures that may affect the antenna

DOI: 10.54254/2755-2721/2026.LD36578

response. Hence, separation distances should be treated as set-up-specific guidance rather than universal design limits.

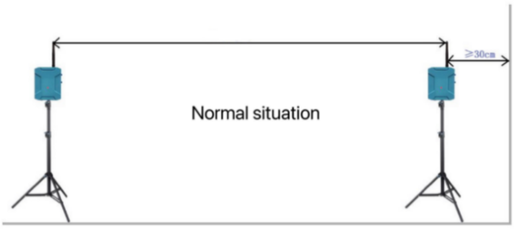

Figure 22. Normal path situation

Figure 23. Indoor with multi-path situation

5.2. Observations and testing with qualitative obstacle-blockage

Figure 24 shows three arrangements of blocks. In Figure 24, when we place a wooden board between test probes, communication is effective. In Figure 25, when metal plate is placed between test probes, communication is still effective, but the performance is highly degraded. However, in Figure 26, reliable operation was not obtained through the tested concrete wall. These results should not be considered into material-penetration limits because the obstacle dimensions, probes separation, radio configuration, trial count, and measurement errors were not fully recorded. However, they show the need for anchor redundancy in indoor deployments [12]. If any anchor is blocked, it could be detected through measurements of timestamp consistency, received-signal diagnostics, or assigned a lower weight by the localization algorithm.

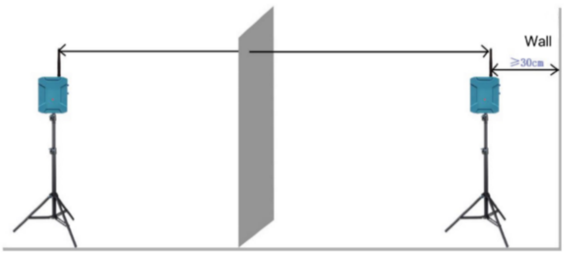

Figure 24. Test with wooden block

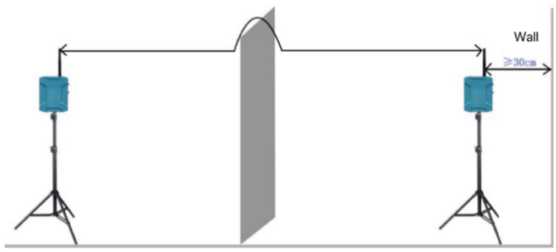

Figure 25. Test with metal plate

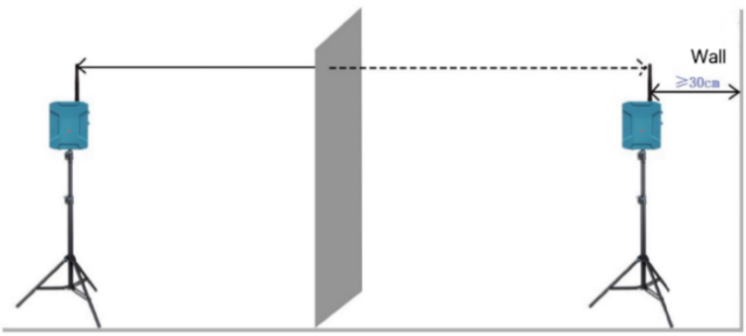

Figure 26. Test with wall

DOI: 10.54254/2755-2721/2026.LD36578

5.3. The orientation of antenna and wireless activity

The orientation of the antenna also affected the system performance. In the configuration for testing, both the horizontal and vertical orientations are tested, placing the antenna horizontally relative to the ground resulting in more stable operation than the vertical orientation. This might be because of polarization alignment, the antenna radiation pattern, and coupling with the ground plane or vehicle structure [13]. In this case, a consistent orientation shall be maintained across different anchors, and the final placement on the platform shall be verified before final integration. The stability also reduces while the platform approaches active Wi-Fi equipment. However, because wireless channel, transmit power, separation, etc. haven't been well controlled, this observation does not establish a direct RF interference.

6. Conclusion

This paper presented a configurable DW1000-based hardware platform for future multi-anchor TDoA localization. The design addresses the fixed antenna, predefined PCB layout, and limited external interfaces of the commercial modules used in the previous study. It provides dedicated anchor and tag layouts, an STM32 controller, controlled RF routing, and a wired interface for timestamp and measurement transfer.

Three antenna candidates were modelled in CST using the same 1.2-mm F4B substrate and simulation conditions. The modified circular antenna provided the widest preliminary -6 dB range, approximately 6.0313-6.4318 GHz, compared with 310.0 MHz and 224.0 MHz for the conventional circular and rectangular patches. It was therefore selected as the initial PCB candidate, although further optimization is required to achieve a satisfactory −10 dB operating band.

A three-layer firmware structure was developed for the system. An infrared-synchronized ultrasonic unit was added for short-range bias testing and initial estimation. However, this measurement only reduces the possible initial-position region. It cannot independently calculate a two-dimensional position or correct the clock drift between anchors.

The qualitative tests showed that performance became worse with wooden, metal and concrete obstacles. In the tested arrangement, horizontal antenna placement was more stable. These observations still require controlled quantitative experiments. Future work will include PCB fabrication, antenna measurement, anchor synchronization, multi-anchor TDoA testing and position-error analysis.

References

[1] IEEE SA Standards Association. (2020). IEEE standard for low-rate wireless networks--Amendment 1: Enhanced ultra wideband (UWB) physical layers (PHYs) and associated ranging techniques. https://standards.ieee.org/ieee/802.15.4z/10230/
[2] Rao, Y., Wen, K., & Brennan, P. (2026). Time difference of arrival localization based on ultra-wideband: A synergistic method of system and algorithm. *Applied and Computational Engineering, 255*, 15-26.
[3] Decawave Ltd. (2024). Sources of error in DW1000-based two-way ranging (TWR) schemes, application note APS011.
[4] Decawave Ltd. (2017). DW1000 datasheet, version 2.22. https://www.qorvo.com/products/d/da007946
[5] Zhao, S. L., Guo, X., Gu, B., & Tian, X. (2025). Non-cooperative UWB base station position estimation method in indoor environments. *2025 IEEE International Conference on Cloud Computing Technology and Science (CloudCom)*, Shenzhen, China, 1-6.
[6] Balanis, C. A. (2016). *Antenna theory: Analysis and design* (4th ed.). Wiley. pp. 783-815.
[7] Pozar, D. M. (2012). *Microwave engineering* (4th ed.). Wiley. pp. 48-85.

DOI: 10.54254/2755-2721/2026.LD36578

[8] Decawave Ltd. (2016). *DW1000 software API guide* (Version 2.7). pp. 1-101. https://forum.qorvo.com/uploads/default/original/1X/8b220e1e26fea4ebd83f0b0e5ef42eb9a251310d.pdf
[9] Carotenuto, R., Iero, D., Pezzimenti, F., Della Corte, F. G., & Merenda, M. (2021). Ultrasonic ranging using frequency selective attenuation. *2021 IEEE International Ultrasonics Symposium (IUS)*. Xi'an, China. pp. 1-4.
[10] Decawave Ltd. (2024). *Antenna delay calibration of DW1000-based products* (Application Note APS013). https://www.qorvo.com/products/d/da008447
[11] Schmidt, S. O., Cimdins, M., John, F., & Hellbrück, H. (2024). SALOS—A UWB single-anchor indoor localization system based on a statistical multipath propagation model. *Sensors, 24*, 2428.
[12] Zang, N., Chen, S., Cheng, J., Zhao, G., & Cai, R. (2026). A fuzzy-logic-enhanced multimodal NLOS mitigation approach for robust PPP/INS/UWB seamless positioning system in observability-deteriorated environment. *IEEE Internet of Things Journal, 13*(1), 918–934.
[13] Grasso, P., Innocente, M. S., Tai, J. J., Haas, O., & Dizqah, A. M. (2022). Analysis and accuracy improvement of UWB-TDoA-based indoor positioning system. *Sensors, 22*, 9136.